Fermi National Accelerator Laboratory

FERMILAB-Pub-87/216-E
[E-740]

Hadron and Electron Response in a Uranium Liquid Argon Calorimeter from 10-150 GeV*

S. Aronson, H. Gordon, W. Guryn
Brookhaven National Laboratory, Upton, NY 11973

P. Franzini, P. M. Tuts
Columbia University, New York, NY 10027

B. Cox, N. Giokaris[a], H. Greif[b], A. Ito
A. Jonckheere, P. Mazur
Fermi National Accelerator Laboratory, Batavia, Il 60510

T. Marshall, A. Zieminski
Indiana University, Bloomington, IN 47405

S. Cantley, D. Owen, B. G. Pope,
S. Stampke[c], H. Weerts
Michigan State University, East Lansing, MI 48824

J. Sculli
New York University, New York, NY 10003

E. Gardella, W. Kononenko, W. Selove, G. Theodosiou
University of Pennsylvania, Philadelphia, PA 19104

T. Ferbel, F. Lobkowicz, E. Prebys
University of Rochester, Rochester, NY 14627

P. D. Grannis, S. Linn[d], M. Marx, R. D. Schamberger
State University of New York, Stony Brook, NY 11794

November 1987

*Submitted to Nucl. Instrum. Methods A

HADRON AND ELECTRON RESPONSE IN A URANIUM LIQUID ARGON CALORIMETER FROM 10 - 150 GEV

Authors

S. Aronson, H. Gordon, W. Guryn
Brookhaven National Laboratory, Upton, NY 11973, USA

P. Franzini, P.M. Tuts
Columbia University, New York, NY 10027, USA

B. Cox, N. Giokaris [a], H. Greif [b], A. Ito, A. Jonckheere, P. Mazur
Fermi National Accelerator Laboratory, Batavia, IL 60510, USA

T. Marshall , A. Zieminski
Indiana University, Bloomington, IN 47405, USA

S. Cantley, D. Owen, B.G. Pope, S. Stampke [c], H. Weerts
Michigan State University, East-Lansing, MI 48824, USA

J. Sculli
New York University, New York, NY 10003, USA

E. Gardella, W. Kononenko, W. Selove, G. Theodosiou
University of Pennsylvania, Philadelphia, PA 19104, USA

T. Ferbel, F. Lobkowicz, E. Prebys
University of Rochester, Rochester, NY 14627, USA

P.D. Grannis, S. Linn [d], M. Marx, R.D. Schamberger
State University of New York, Stony Brook, NY 11794, USA

Abstract

A uranium liquid argon calorimeter, with a total depth of nine absorption lengths, has been exposed to electrons and hadrons in the energy range of 10 - 150 GeV. Two configurations with different uranium plate thicknesses were successfully operated. In both cases the response was found to be linear over the entire energy regime. We present measurements of various contributions to energy resolution, differences in electron/hadron/muon response, longitudinal and transverse shower profiles and electron position resolution.

a) Now at The Rockefeller University, New York, N.Y. 10021
b) Visitor from Max Planck Institute, Munich, West Germany.
c) Now at the University of Notre Dame, Notre Dame, Indiana 46556
d) Now at Florida State University, Tallahassee, Florida 32306

(submitted to Nuclear Instruments and Methods)

1. Introduction

The D0 detector, planned for the study of $p\bar{p}$ collisions at a center of mass energy of 2 TeV at Fermilab, requires very good jet energy resolution and shower containment. In order to achieve these goals an equalization of the electron and hadronic response of the calorimeter, as well as high density, are needed. At low energies, uranium liquid argon calorimeters have been shown to have such characteristics.[1] This and the compactness, uniformity of response, and radiation hardness that can be achieved make uranium and liquid argon the choice for the D0 experiment. The present study was designed to measure the response of a prototype calorimeter to both electrons and hadrons (the beam polarity was negative, so the majority of what we call hadrons were pions) in the energy range 10 - 150 GeV and to explore the options for final design relating to uranium plate thickness, longitudinal and transverse segmentation and uranium induced noise.

2.Calorimeter set-up

A test calorimeter was constructed to measure the properties of electron and hadron response. It consisted of a twenty radiation length (X_0), fine sampling, electromagnetic section followed by a five absorption length (λ) fine hadronic section. These sections used uranium as absorber, and were followed by a three absorption length leakage section, where copper was used instead of uranium. Two different uranium plate thicknesses were tested in configurations labelled Load II and Load III. Load II used 2 mm and 4 mm thick uranium for electromagnetic and fine hadronic section absorber plates respectively; Load III had uranium plates two times as thick as Load II. Table I describes the different longitudinal segmentations used. The active transverse size of the calorimeter was 60 cm by 50 cm, with the absorber plates being slightly oversized (60 cm by 60 cm). The ionization electrons were collected by signal boards located in the middle of the gap between absorber plates. The unit cell consisted of: absorber-1.6 mm Ar-1.6 mm signal board-1.6mm Ar-absorber. The signal boards were made of double copper-clad G10, with

a pad-pattern etched on them as shown in Figure 1. There were forty-eight pads per board. As indicated in Table I the three main sections were subdivided further, such that each segment consisted of the sum of several argon gaps . Each segment was read out in an interleaved fashion, with odd and even numbered gaps added separately. This enabled us both to measure two absorber thicknesses in one load and also to study the impact of shower fluctuations on the resolution. Thus the number of signals per segment was 96. The interleaving readout scheme was only employed in the uranium parts of the calorimeter. In Load II the coarse hadronic section was transversely ganged in such a way that only 18 signals were read out. During Load III, however, all pads from this section were read out, but the first two sections of the electromagnetic section were not interleaved. This resulted in a total of 690 channels in Load II and 672 in Load III. In addition to these there were 48 more channels from a signal board that did not have an argon gap. This served as a monitor for noise pickup. The capacitances for the readout channels were in the range 0.1-1.3 nF for the electromagnetic section and 0.5-5.5 nF for the fine hadronic section.

Typical signals at the charge collecting pads were of the order of 0.1 pC per GeV of total energy deposit in the calorimeter. These minute charges, collected on the above mentioned capacitances, were measured with charge sensitive pre-amplifiers[2]. Signals from the calorimeter stack were carried via 3-4 m long twisted pair cables to a feed-through and from there via a short twisted pair cable (.5-.75 m) to the preamps, which were housed in a shielded preamp box, attached to the cryostat. This is shown schematically in Figure 2. The pads were a.c.-coupled to the preamp inputs and were kept at ground potential by two protection diodes at the preamp input. High voltage applied to the absorber plates provided the drift field for charge collection. Signal ground return was via 0.1 μF capacitors for each absorber plate. This arrangement was the simplest mechanically, but introduced cross talk of opposite sign from a pad with signal to all other pads in the same

gap. The sum of all cross talk signals was a fraction of the true signal given by the ratio of the gap capacitance to the capacitance of the blocking capacitor and was about 6% in our case. In cases where one wants to add many pads, or use signals at the edge of the shower for position determination a small correction can be made. In many cases this effect can be neglected. It is however straightforward to correct for it. For the input stage of the preamps we used Toshiba (type 2SK147) field effect transistors which gave, for large capacitances of the signal source, a factor of 2 to 4 lower noise than previously obtainable with this low power consumption and low cost. With these preamps we obtained satisfactory noise performance without the use of step up transformers. (For details on noise, see Appendix A). The preamp output signals were mildly differentiated (50 μs), integrated to remove high frequency FET white noise with an RC constant of 0.5 μs and double sampled (before and after the signal) with an interval of 3.5 μs as shown in Figure 2. The difference of the two samples, obtained with an operational amplifier, was digitized by a commercial ADC unit (LeCroy model 2249A). The sensitivity of the system was one digitizer count for 4500 input electron charges. This resulted in a response of 4.2 counts per MeV of energy lost in argon, using the standard value of one collected electron charge per 52 eV of energy deposited in liquid argon.

The cryostat was filled with argon from several dewars. In order to avoid purity problems, every bottle was checked with a test cell before it was used. The test cell consisted of a 1.35 mm argon gap, with an ^{241}Am source mounted on one side. The charge liberated by the emitted α's was measured as a function of the applied drift field and compared with standard curves[1]; no bottle needed to be rejected. To monitor the purity within the calorimeter cryostat an identical test cell was placed inside; an oxygen-monitor also sampled the argon gas in the cryostat. Despite these precautions, the first fill of argon in the cryostat was contaminated in such a way that it was not possible to establish a high voltage plateau for 50 GeV electrons or pions. Despite chemical analysis of the gas

samples, the source of the impurity was not clearly established; but dumping the argon and refilling solved the problem. In all the running after this incident, even after opening; closing and refilling the cryostat, impurities caused no problems and the oxygen level was of the order of 2-3 ppm.

3. Analysis of the Data

The two calorimeter loads were exposed to electrons and pions from the NW-beam at Fermilab (negative polarity) in the energy range 10-150 GeV. The beam line was operated in slow spill mode and the particle rate was limited to about 500/sec to avoid pile-up of events. In addition to this low rate there was a veto, which inhibited the trigger if the time between beam particles was less than 1 ms. To establish the operating voltage of the calorimeter, 50 GeV electrons and pions were used; Figure 3 shows the voltage dependence of the collected signal. Based upon these results, 1500 V was chosen as the operating voltage for all further running, which corresponds to 943 V/mm drift field in the gap.

For analysis of the data the following procedures and corrections were employed:

a) For each channel, the pedestal value and the width of the distribution were determined by a special pedestal trigger. Such triggers were intermixed with the data during the beam spill, as well as taken outside the beam spill, to look for any beam dependent effects. None were observed. During analysis, a running average of the pedestal was kept and used as pedestal subtraction for each individual channel.

b) To determine the relative channel-to-channel calibration, a fixed pulse was injected into each channel at the preamp stage via a precision resistor, whose resistance was accurate to 0.1%.

c) Dead or shorted (pad to absorber) channels could be easily identified by an abnormally wide pedestal distribution or by failure to respond to the charge injection system. They were corrected by replacing their contents with the signal measured in their interleaved counterpart. Typically 1 to 2 channels had to be corrected for a run and in 95% of the cases the channels were in non-crucial locations in the calorimeter.

Due to the different thicknesses of absorber used in the different parts of the stack, energy observed in them has to be weighted before signals from different sections can be added together to give the total signal for a shower. This was done by weighting each section by its sampling fraction (SF). The sampling fractions used are given in Table I and were derived from dE/dx properties of the materials used. For a given section the sampling fraction was defined as:

$$SF = \frac{dE}{dx_{Ar}} \Big/ \left(\frac{dE}{dx_{Ar}} + \frac{dE}{dx_{G10}} + \frac{dE}{dx_{absorber}}\right) \qquad (1)$$

where dE/dx is the mean energy lost by a minimum ionizing particle (MIP). Each signal was weighted as:

$$PH = \frac{ADC - PED}{GAIN \times SF} \qquad (2)$$

where SF is that appropriate for the particular section, PED the pedestal for that particular channel, ADC the measured signal before any corrections and GAIN the relative channel to channel gain correction.

4. Energy response of electrons and hadrons

All results for pulse height (PH) are given in counts, with corrections for all of the above mentioned effects. In the subsequent discussion of the calorimeter response, in the case of hadrons all channels (all three sections) and for electrons all channels in the

electromagnetic section were added to obtain PH. However only a fraction of the total channels contain real energy and all of the empty channels just increase the spread of the distribution. We attempted to reduce this effect through elimination of empty channels by summing only channels where $|PH_i| > 1.5\sigma_i$. Here σ_i is the RMS of the pedestal distribution for channel -i-. A symmetric cut such as this, which retains large positive as well as negative excursions was necessary to keep the response linear. A simpler cut, only keeping channels where $PH_i > 1.5\sigma_i$ for example introduced a 20% non-linearity below 25 GeV and therefore could not be used. Results are presented here with ("1.5 σ cut") and without this noise reduction cut ("no cut").

Due to long ground return loops in Load II there was substantial cross-talk between different sections whenever energy was deposited in the device. A cross-talk matrix was measured by taking data with individual sections switched off and this matrix was then used to correct the pulse height from each section before summing them. This procedure corrected all the central values but did not eliminate contributions to the widening of the signal. Because of this correction the above mentioned noise suppression technique could not be applied in Load II, because empty channels behave differently during data taking and during pedestal runs. In Load III the problem was fixed and within our accuracy no cross-talk between sections could be measured. The channel-to-channel cross-talk of neighboring channels was measured to be of order one part in ten thousand.

Figure 4 shows the linearity of the device; Fig. 4a shows the pion and electron response for Load II; Fig. 4b gives the results for Load III with and without noise suppression. We plot here the quantity PH divided by the beam energy as a function of the beam energy. Without any noise cuts both loads show the same behavior, namely a 1 to 2% non-linearity below 25 GeV. With the removal of empty channels the magnitude of the result remains the same but now the sign of the non-linearity has changed. It is our belief

that this non-linearity arises from a combination of residual noise and the energy-summing algorithm and not from an intrinsic non-linear response at these energies. We have verified that this change is due to a small asymmetry in the pedestal distributions, which for all purposes had been considered symmetric. It should be noted that no 10 GeV hadron data were available with the Load III stack.

The fractional energy resolution (σ/E) was determined for the different loads, particles and cuts and is given in Table II and shown in Figures 5 and 6. Here σ was obtained from fitting a Gaussian to the complete pulse height spectrum at every energy without any cuts. An example of such a spectrum for 25 GeV electrons and hadrons is shown in Figs. 7a and b. This procedure for obtaining σ ignores tails and only takes into account the central part of the distribution. Figure 5 shows σ/E plotted as a function of $1/\sqrt{E}$ for electrons in Loads II and III without any cuts. The resolution is expected to be linear in $1/\sqrt{E}$ if only sampling fluctuations play a role and is expected to scale with the square root of the absorber thickness. The comparison of the two data sets in Fig. 5a clearly shows that there are additional terms contributing to the measured resolution. One effect present only in Load II is due to variations in the cross-talk and contributes a constant term to the fractional resolution. This is clearly seen at the higher energies where the data without such problems and a thicker absorber (Load III) result in a better resolution. An additional contributor to the resolution is noise which causes deviations from linearity in $1/\sqrt{E}$. This is clearly demonstrated by Fig. 5b where the removal of empty channels gives a result in better agreement with a linear behavior than the one without empty channel suppression. In view of the different sources contributing, the resolution was fitted to the form:

$$(\frac{\sigma}{E})^2 = A^2 + (\frac{B}{\sqrt{E}})^2 + (\frac{C}{E})^2 \qquad (3)$$

Here A accounts for intrinsic inaccuracies (e.g. relative channel calibrations)in the

calorimeter, B measures the contribution from shower fluctuations and C determines the contribution from electronics and uranium noise sources (see also Appendix). The results from the fits are displayed in Table III. Only results for Load III are given because of the above mentioned cross-talk problems in Load II. In these fits the contribution due to the finite beam momentum spread(1.2-1.5%) was taken into account and is not therefore included in the estimate for A. Resolution broadening due to energy fluctuations in upstream inert material (cryostat walls for example) were not accounted for and do contribute to the resolution. The total amount of upstream material is about $1.2X_0$. The C term, in the case of Load III, can also be determined independently from the pedestal data. The value for C found that way compares well with the result from the fit to the resolution..

The same procedure as for electrons was also employed for hadrons and the results are shown in Figures 6a and 6b. Because of the larger values for the resolution, the cross-talk problem in Load II is not apparent when both data sets are compared. Again the contribution of noise to the resolution is very apparent at the lower energies as is illustrated in Fig. 6b, by comparing data with and without the noise cuts. The flattening of the resolution above 75 GeV is due to the intrinsic resolution of the device resulting from channel to channel variations and from the different response of the calorimeter to the pure electromagnetic and hadronic components of the hadronic shower.[3] Also the effect of back leakage may manifest itself at the higher energies. The same fits as in the electron case were performed and the results displayed in Table III. Also in this case the determination of the C-term from the resolution fits agrees very well with the independent determination in the Appendix. All these hadron resolutions were obtained with the standard weighting of the individual sections as outlined above. Different weighting schemes of individual sections or groups of sections, as successfully applied in other calorimeters [4], were tried. The weights were determined by minimizing the resolution, but with our longitudinal segmentation no significant overall improvement could be

achieved. The best that could be done was a 5% improvement at certain energies, but at the cost of introducing a non-linear response. Simple dE/dx weighting is completely satisfactory for this device.

Figure 8 shows the containment and hadron resolution as a function of calorimeter depth used for 15, 25 and 100 GeV incident particles. For the employed configuration seven absorption lengths were sufficient to contain enough of the shower, so that the resolution does not improve by more than 2% if a thicker calorimeter is used. It should be noted however that our fine sampling also stopped after six absorption lengths.

One crucial requirement for obtaining a good hadron resolution is the equalization of the hadronic and electromagnetic response of the calorimeter. Figure 9 shows the measured ratio of the electron over the hadronic response (e/h) as a function of energy. For both loads this quantity is practically energy independent, although a 2 to 3% rise at lower energies in Load II cannot be excluded. The statistical errors on the data are on the order of the size of the data points. The average values assuming an energy independent response are 1.13±.02 for Load II and 1.11±.01 for Load III where the errors are purely statistical. A possible over-estimation of the ratio is caused by hadronic energy leaking out the sides of the detector. From preliminary fits to the transverse profiles of hadronic showers this systematic error was estimated to be at most 2% for both loads. This approximate equalization of the hadronic and electromagnetic response in a liquid argon detector is believed to be due to a suppression of the electromagnetic shower component and any boost of the hadronic signal due to fission and spallation is expected to be small[3].

In order to compare the response of the calorimeter to electromagnetic showers with the response to minimum ionizing particles the ratio:

$$\frac{\mu}{e} = \frac{PH_{\mu}}{E_{\mu}} \frac{E_{elec}}{PH_{elec}} \qquad (4)$$

was determined. Here PH are the measured pulse heights for muons and electrons and E the beam energy in the case of the electrons; in the case of the muon it is the total energy the muon loses by traversing the electromagnetic section of the calorimeter. All quantities except E_μ were measured.The muon data were obtained during the hadron running and the most probable value of the pulse height distribution was determined, from which the mean pulse height was calculated assuming a Landau distribution. The resulting values depend on the value of E_μ. If one assumes that the muon behaves as a minimum ionizing particle (MIP) whose energy loss is given by the dE/dx tables in Review of Particle Properties [5], we obtain $\mu/e = 2.1 \pm 0.2$ at 25 GeV and 2.0 ± 0.2 at 50 GeV. If the relativistic rise in the ionization loss of the muon is taken into account [6], which is only significant in uranium , we obtain $\mu/e = 1.4 \pm 0.1$ and 1.3 ± 0.1 at 25 GeV and 50 GeV respectively. These results show that the charge collected from the argon per unit energy deposited in the calorimeter is different for muons and electrons, but one has to keep in mind that the muon, during this process, loses practically no energy whereas the electron loses all of its energy and most of the energy deposition is in the form of low energy electrons whose energy loss characteristics are very different. The above ratio was also determined at the other available energies and shows no energy dependence within the experimental errors.

The electron response was more directly checked by comparing the signal obtained at 50 GeV with the expected charge collected from the argon. Using an absolute calibration of the readout system and using 1.89 10^4 e's/Mev as the electron yield in argon for conversion of beam energy to expected signal, it was found that the measured sampling fraction was 3.78%. The sampling fraction expected from dE/dx using [5] is 7.2%, which results in a ratio of 1.91. This ratio of measured and expected sampling fractions, which should be the same as μ/e, indeed agrees very well with the result for μ/e where the same dE/dx for the muon from ref.[5] was assumed.

5.Longitudinal profiles of electrons and hadrons

The electromagnetic section of the calorimeter was subdivided into 4 depth segments (see Table I) in order to enable good electron-hadron separation and good position resolution for electrons. Figure 10 displays electron shower longitudinal profile data from Load III. Statistical errors are generally smaller than the points. Electrons giving evidence of hard radiation in the beam were removed from the sample by cuts on total energy deposited and impact point residual. A small hadron contamination was removed by requiring no energy deposit in the hadronic sections.

Due to the coarse, depth dependent segmentation we calculated ratios, $R_i = \langle E_i \rangle / \langle E_e \rangle$, where E_i is the energy deposit in segment i and E_e is the total observed deposit . "Leakage" into the first fine hadronic segment(FH1) is small, increasing slowly to less than 2% at 150 GeV. Above about 25 GeV, the shower maximum is inside the third electromagnetic segment(EM3) resulting in nearly energy independent ratios for that section.

The Longo and Sestili[7] parameterization for the mean electromagnetic longitudinal shower shape,

$$\frac{dE}{dt} = At^{\alpha}e^{-bt} \tag{5}$$

where t is the shower depth in X_0, successfully describes our data. To find α and b, we must respect the depth segmentation,

$$\langle E_i \rangle = A \int_{T_i}^{T_{i+1}} t^{\alpha}e^{-bt}\, dt \tag{6}$$

where T_i and T_{i+1} are the limits of section EM_i.

T_1, the start of EM_1, accounts for inert material in the cryostat and beamline upstream of the detector. Estimates gave about $.1X_0$ in the beam and $1.1X_0$ in the cryostat. Our fits to the data of Figure 10 allow 1.0 to 1.35 X_0 for the total upstream material. While

little energy (on average about 90 MeV) is deposited upstream, the shower shape within the detector is sensitive to this loss. Ignoring it is incompatible with our data.

The energy dependence of the parameters α and b was established with fits to the ratios of Figure 10 at each individual energy. The points of Figure 11 are α and b from these single energy fits (with $T_1 = 1.02X_0$, see next paragraph). They indicate

$$\alpha = \alpha_0 + \alpha_1 \ln E \qquad (7)$$
$$b = b_0 + b_1 \ln E$$

where E is in GeV and b_1 is essentially equal to zero. α_0 and α_1 were somewhat sensitive to the assumed value of T_1. However the logarithmic rise in α with energy was found with all values of T_1 tried.

For further analysis we made a global fit using all energy values and sections through FH1. Parameters were α_0, α_1, b_0, b_1, and T_1. We found it necessary to include a systematic error term, ε, added in quadrature with the statistical errors:

$\sigma^2_i = \sigma^2_{i,stat} + (\varepsilon R_i)^2$. With $\varepsilon = .0016$, our results are

$$\alpha_0 = 1.565 \pm 0.97 \qquad \alpha_1 = 0.406 \pm 0.16$$
$$b_0 = 0.492 \pm 0.12X_0^{-1} \qquad b_1 = -.006 \pm .002X_0^{-1} \qquad (8)$$
$$T_1 = 1.02 \pm .07X_0$$

with $\chi^2/dof = 1.07$. The solid lines in figure 10 are from this fit.

If we use only statistical errors, ($\varepsilon = 0$), we do no better than $\chi^2/dof = 5.9$, without FH1 and $\chi^2/dof = 9.7$, with FH1 included in the fit. The first of these fits yields $\alpha_0 = 1.69$, $\alpha_1 = 0.48$, $b_0 = 0.50X_0^{-1}$, $b_1 = 0.0004X_0^{-1}$, and $T_1 = 1.35X_0$. In both cases, FH1 data lie significantly above the fit. After seeking to determine if this FH1 excess was evidence for an extended tail[8] to the shower, we concluded that we have no evidence for an extended tail, and that systematic errors dominate the uncertainties in our data.

To determine electron-pion separation, a method based upon a covariance matrix describing the longitudinal energy deposition[9] was used. With 91% electron acceptance

the pion rejection above 100 GeV is better than 700:1 and decreases to 400:1 at 50 GeV. At lower energies the rejection becomes worse, but it should be noted that no particle identification was available in the beam line and that the electron content of the hadron beam increases at lower energies. Thus the above rejection factors should be viewed as lower limits. Rejection of the same quality was achieved by comparing the fractional energy in the hadron and the electromagnetic segments and requiring the major fraction of the energy to be in the electromagnetic section.

We have attempted to parameterize the mean longitudinal shape of hadron showers as measured in the Load III test calorimeter. A now standard parameterization for fitting hadron shower profiles was developed by Bock et al.[10] Following their analysis, one can describe the longitudinal energy deposition in the calorimeter as:

$$\frac{dE}{dz} \sim w\, t^{-\alpha} e^{-\beta t} + (1-w)\, s^{-\alpha} e^{-\delta s} \qquad (9)$$

where z = calorimeter depth

$t = z/X_0$, number of radiation lengths

$s = z/\lambda$, number of absorption lengths

w = relative weight of the electromagnetic core of the shower (produced by π^0's)

$1-w$ = relative weight of the hadronic part of the shower

In general, the four parameters α, β, δ and w have a logarithmic energy dependence, reflecting the observation that the average center of gravity and attenuation length of showers have a logarithmic energy dependence.

$$\alpha = \alpha_1 + \alpha_2 \ln E \qquad \beta = \beta_1 + \beta_2 \ln E$$

$$\delta = \delta_1 + \delta_2 \ln E \qquad w = w_1 + w_2 \ln E \qquad (10)$$

The six energy samples between 15 and 150 GeV were used to extract the best fit for all 8 parameters. Our values for the parameters are listed in Table IV.

6. Transverse electron profiles and electron position resolution

Transverse profiles of electron showers at normal incidence were studied with Load III data at all energies. Figure 12 gives a qualitative look at a 150GeV transverse shower profile in EM3. In this run the beam, whose projected impact position could be determined to ±0.3mm by upstream wire chambers, was targetted far from the calorimeter axis on a group of leads(.76mm pitch) servicing pads at the calorimeter bottom. These pads were 10 to 20cm from the beam center in this run, so their channels only collected charge from these leads. The leads were exposed to the liquid argon and fully efficient. Figure 12 displays the charge on a single lead as a function of the electron impact position(x_b). This kind of data was only available at two energies and was sensitive to mechanical tolerances as discussed below. The RMS's of these differential profiles at 150GeV were 0.29cm, 0.36cm, 0.43cm and 0.54cm in EM1 to EM4.

A detailed study of the transverse electron profiles (outlined below) at all energies showed that electron showers had a dominant narrow core with a broad tail in the first three depth segments (EM1,EM2 and EM3). In EM3, the 50, 90 and 98% containment regions were typically ±0.3cm, ±1.5cm and ±3cm from the shower axis at all energies. To determine the transverse shape profile systematically we used data with the beam approximately centered in the calorimeter. At all energies and in all electromagnetic segments, the projected differential transverse profiles were consistent with a sum of two exponentials[14]:

$$\frac{dE}{dx} = f(x - x_b) = A_1 e^{-B_1 |x - x_b|} + A_2 e^{-B_2 |x - x_b|} \qquad (11)$$

where x_b is the projected electron impact point, equal to x_s the shower axis. A_1, A_2, B_1 and B_2 are energy and depth dependent parameters. These parameters were determined by fits to the experimental ratio:

$$G(x_b) = \frac{E(x>0)}{E_T} = \frac{\int_0^{\infty} f(x - x_b)dx}{\int_{-\infty}^{\infty} f(x)dx} \qquad (12)$$

Here E_T is the total deposited energy and E(x>0) includes only pads to one side(x>0) of the calorimeter axis. The beam central axis was near the pad boundary at x=0; finite beam size allowed measurement of $G(x_b)$ over a range of about 3cm, extending well into the shower tail. Experimental ratios were accumulated in 1mm bins and then fit to the double exponential shape[15]. This analysis was performed on each electromagnetic depth segment at each available energy between 10 and 150GeV.

Figure 13 shows the experimentally observed $G(x_b)$ distributions for all EM layers at 50 GeV with $x_b = 0$ being the calorimeter axis pad edge. The results of the fit are superimposed and the numerical values for the depth dependence of the parameters are given in Table V. The contribution from both narrow and broad exponentials is apparent. (We should comment that $G(x_b)$, being a ratio of integrals, emphasizes the shower tails.) The core slope parameter B_1 displays a slow broadening with increasing depth, while the tail is little changed through shower maximum in EM3. The energy dependence of the transverse shape parameters is illustrated in fig. 14, which shows the values for EM3. The data suggest that A_2/E_T, B_1 and B_2 are nearly energy independent in this segment. A_1/E_T then reflects the movement of the shower maximum into EM3 for energies above 25GeV.

The transverse shape study had systematic problems, including readout board alignment uncertainties of 0.5mm, a small (14mrad) rotation of the calorimeter, and the capacitive cross talk mentioned earlier. These effects have not been accounted for and contribute to the width of the peak in fig 12. Hadron contamination was eliminated by cuts on energy deposition in the hadronic sections. Upstream bremsstrahlung interactions were present at the few percent level in the data used for the the profile fits. These effects limit

the reliability of the numerical shower shape parameters. In particular B_1 in EM2 and EM3 may be slightly underestimated. However the general features of the shape and the position resolution results we quote below were not affected. For the position resolution study, upstream interactions caused unusually large residuals(the difference between beam impact point and shower position calculated from calorimeter information) and were removed by loose cuts on this residual(3.5 times the 15GeV position resolution).

We have also determined the position resolution at normal incidence, as a function of the distance of electron impact from the pad edge. We used EM3 information only, because the final D0 calorimeter will have a factor of two finer segmentation in EM3 than in the other sections and electromagnetic shower position reconstruction will rely primarily on this section. The aim of our study was to find an algorithm free of any inherent systematic biases and to establish position resolution limits. Several previously suggested algorithms[14,16] were initially tried. Center of gravity calculations were found little better than simply assigning the shower location to the center of the pad with the maximum energy. Methods using a single exponential transverse profile parametrization gave significant distortions in the computed shower position.

The best results were obtained using an intregated shower ratio function $G_3(x)$, defined like G(x) in equation (12), but determined by only using EM3 information for E(x>0) and E_T. The condition:

$$G_3(x_s) = \frac{E_3\ (x>0)}{E_3} \qquad (13)$$

was used to determine the shower axis position x_s, from E_3, the total energy in EM3 and $E_3(x>0)$ the energy on pads with x>0 in EM3. Eq. (13) was used for cases where $x_b<0$ (the true impact point). For $x_b>0$ one would use the complimentary expression $E_3(x<0)$.

The computed shower axis, x_s was compared with the known beam location x_b to give a distribution whose width can be taken as the error in the shower axis location. Systematic errors in x_s were found to be negligible, approaching 1mm only for x_b beyond

2.5cm from the pad edge used in eq. (13). The random position error in the reconstructed shower position as a function of x_b, $\sigma_s(x_b)$, found this way is shown for several energies in fig. 15. In this figure the position resolution is given as a function of distance between the beam impact point and the physical pad edge. As expected the resolution improves as the energy increases. Note that over most of our 5cm pads, the position resolution is dominated by fluctuations in the neighboring pad and this is well into the tail for showers whose axis is more than a few millimetres from the pad edge. A rough parametrization of the position resolution $\sigma_s(x_b)$ for E>10GeV is:

$$\sigma_s(x_b) = (.01 + \frac{.34}{\sqrt{E}}) + (.03 + \frac{.85}{\sqrt{E}})\ |x_b| \quad [\text{cm}] \qquad (14)$$

where $|x_b|$ is again the distance between pad edge and beam impact point and E is the electron energy in GeV. It should be noted that (14) is based upon a "single edge" calculation i.e. only pads to one side (either x<0 or x>0 in eq. (13)) were used. One could do a "double edge" calculation by using eq. (13) for both edges of a pad(on either side of the shower) and using the weighted average as the best estimate of x_s .Average position resolution as a function of pad size can be estimated by averaging eq. (14) over the selected pad area. For a 5cm pad in our test calorimeter, illuminated uniformly, the average position resolution using this "single edge" reconstruction(with the edge nearest to x_b) is 0.5cm at 15GeV and 0.2cm at 100GeV. A double edge reconstruction improves this by only 13%. In both cases the position uncertaintity decreases with energy roughly as $E^{-0.4}$ in the energy range studied.

This "single edge" reconstruction procedure is viewed only as a prototype for final electron position reconstruction. It was used here to provide an algorithm without reference to pad sizes. However the calculation points out the need to respect the correct mean shower shape to remove systematic effects and the role of shower fluctuations in limiting the position resolution.

We wish to acknowledge the help of the Research Division, the Accelerator

Division and the Physics Department of Fermilab in the execution of these tests. Especially important was the work of Delmar Miller, Mike Nila, George Mulholland, and Kurt Krempetz from FNAL and Sharon Joy and Ron Richards from MSU. David Anderson participated in helpful and stimulating discussions. The support of the Department of Energy and the National Science Foundation for the various universities involved in the D0 collaboration is gratefully acknowledged. The interest and help of institutions outside of this collaboration, in particular the Max Planck Institute of Munich and the University of Wisconsin, is acknowledged. Finally, we thank W. Willis and C. Fabjan of CERN and I. Mannelli of Pisa for assistance, helpful comments and the loan of equipment.

TABLE I

Description of longitudinal segmentation of calorimeter Loads. Material dependent parameters were taken from Ref. [5].

	ELECTROMAGNETIC SECTION	HADRONIC SECTION	LEAKAGE SECTION
	LOAD II		
Absorber:	2 mm Uranium	4 mm Uranium	19 mm Copper
Number of plates:	30	112	24
Argon Gap	3.2 mm	3.2 mm	3.2 mm
Signal Boards (in center of Argon gap)	1.6 mm	1.6 mm	1.6 mm
Sampling fraction:	.129	.072	.026
Thickness:	19.7 X_0	5 λ	3.2 λ
Subdivisions:	1. 2.6 X_0	1. 1λ	1. 1.6λ
	2. 2.6 X_0	2. 3λ	2. 1.6λ
	3. 5.3 X_0	3. 1λ	
	4. 9.2 X_0		
No. of Channels	384	288	18
	LOAD III		
Absorber	4 mm Uranium	8 mm Uranium	19 mm Copper
Number of Plates	16	56	24
Argon Gap	3.2 mm	3.2 mm	3.2 mm
Signal Boards	1.6mm	1.6mm	1.6mm
Sampling Fraction	.072	.038	.026
Thickness	20.8 X_0	4.7 λ	3.2 λ
Subdivisions	1. 2.6 X_0 (EM1)	1. 1.0λ (FH1)	1. 1.6λ (CH1)
	2. 2.6 X_0 (EM2)	2. 2.7λ (FH2)	2. 1.6λ (CH2)
	3. 5.2 X_0 (EM3)	3. 1.0λ (FH3)	
	4. 10.4 X_0 (EM4)		
No. of Channels	288	288	96

TABLE II

Measured energy resolutions (σ/E) for electrons and hadrons. Quoted results were obtained by fitting a gaussian to the total measured spectrum without any cuts.Errors given are statistical only and are insensitive to the different cuts made.

Electrons (σ/E) Load III

Energy [GeV]	No cuts	1.5σ cut	Interleave difference	
			No cut	1.5σ cut
10	.108 ± .003	.078	.064	.054
15	.076 ± .001	.062	.050	.043
25	.052 ± .002	.046	.040	.032
50	.035 ± .001	.032	.030	.026
75	.027 ± .001	.027	.025	.021
100	.025 ± .001	.025	.025	.021
150	.022 ± .001	.022	.023	.019

Hadrons (σ/E)

Energy	Load II	Load III			
[GeV]	No cuts	No cuts	1.5 σ cut	Interleave difference	
				No cut	1.5 σ cut
10	.268	-			
15	.183	.212 ± .003	.178	.128	.111
25	.124	.157 ± .003	.132	.100	.088
50	.077	.099 ± .002	.094	.075	.070
75	-	.075 ± .002	.073	.061	.061
100	.061	.070 ± .002	.070	.054	.050
150	.050	.068 ± .002	.066	.041	.039

TABLE III

Results of fits to the electron and hadron energy resolutions in both loads using:

$$(\frac{\sigma}{E})^2 = A^2 + (\frac{B}{\sqrt{E}})^2 + (\frac{C}{E})^2$$

Data description	Fit number	χ^2/dof	A	B [$GeV^{0.5}$]	C [GeV]
Load II hadrons	1	2.4	.040±.004	.34±.05	2.38±.13
no cuts					
Load III hadrons:					
no cuts	2	4.0	.05±.01	.45±.08	2.7±.2
1.5σ cut	3	1.2	.05±.01	.48±.06	1.8±.3
difference in interleaves	4	5.1	.03±.01	.44±.01	0.0±7.5
1.5σ cut					
Load III electrons:					
no cuts	5	0.9	.016±.002	.17±.02	.90±.06
1.5σ cut	6	0.7	.015±.002	.19±.02	.52±.08
difference in interleaves	7	0.2	.019±.001	.15±.02	.27±.11
1.5σ cut					

TABLE IV

Results of fit to the longitudinal hadron shower development using parametrization from Ref. [10].

Energy Range: 15 to 150 GeV	
$\alpha_1 = 0.34 \pm 0.12$	$\alpha_2 = 0.81 \pm 0.02$
$\beta_1 = 0.30 \pm 0.02$	$\beta_2 = -0.06 \pm 0.02$
$\delta_1 = 0.70 \pm 0.02$	$\delta_2 = 0.09 \pm 0.02$
$w_1 = 0.36 \pm 0.02$	$w_2 = -0.007 \pm 0.009$
$\chi^2 = 6.41$	

TABLE V

Results of fitting double exponentials to the transverse electron shower profiles at 50GeV electron energy. Fitted parameters are given for each electromagnetic segment.

$$\frac{dE}{dx} = f(x - x_b) = A_1 e^{-B_1 |x - x_b|} + A_2 e^{-B_2 |x - x_b|}$$

Segment	A_1 [GeV/cm]	B_1 [cm^{-1}]	A_2 [GeV/cm]	B_2 [cm^{-1}]
EM1	10.04±1.44	7.42±1.31	0.75±0.15	1.16±0.09
EM2	18.34±0.91	4.73±0.16	1.86±0.18	1.19±0.04
EM3	25.70±1.18	3.53±0.14	4.36±0.18	1.02±0.02
EM4	6.58±0.48	1.76±0.31	0.91±0.57	0.54±0.13

Appendix: Electronic and Uranium noise

The noise in the various loads used was studied extensively in order to be able to predict accurately the behavior of the calorimeters in the D0-experiment. The three contributions to the noise that play a role are: incoherent and coherent electronic noise and uranium noise, the latter being caused by the natural radioactivity of the uranium absorber plates. This last noise component could be switched off by switching off the operating voltage and its presence could be easily verified by comparing the copper sections with the uranium sections. The noise in the uranium part clearly rose with increasing high voltage and reached a plateau, whereas it was independent of the operating voltage in the copper section. As a measure of the noise we used the RMS of the pedestal distribution in either a single or in many channels.

To determine the random electronic noise, which is expected to increase linearly with the detector capacitance, the noise in each channel was measured and plotted as a function of the channel capacitance (defined by the cell geometry). This was done with the operating voltage turned off, so uranium noise was not present. Coherent electronic noise plays a negligible role on a per channel basis because of its small magnitude. Figure A1 displays the noise averaged over many channels as a function of the capacitance and these data were fitted with:

$$\sigma_{el} = (.63\pm.02 + .33\pm.02\ C) / SF \quad [MeV] \qquad (A1)$$

Here C is the detector capacitance in [nF] and SF the sampling fraction of the particular calorimeter section. The 50 GeV electron data was used to convert from counts to energy. This result is to be compared with a noise prediction of [11]:

$$\sigma_{pred} = 2000 + 3500\ C \quad [electrons]. \qquad (A2)$$

By using the electron yield in argon of 1.89×10^4 e's/MeV and the fact that electrons (and

hadrons) only yield half this number, as illustrated by the result presented above: $\mu/e = 2.0$, Equation A2 can be written as:

$$\sigma_{pred} = (.22 + .38\ C) / SF \qquad [MeV] \qquad (A3)$$

Thus experiment (A1) and prediction (A3) agree well in the slope. The large disagreement in the intercept is due to the fact that in the measurement cable capacitances were not included in the detector capacitance. Using equation (A1) the total incoherent electronic noise in the individual sections was: electromagnetic-section: 167 MeV, fine hadronic: 413 MeV, leakage: 375 MeV and total calorimeter: 582 MeV.

The noise component due to the use of uranium (σ_U) was determined as follows:

$$\sigma_U^2 = \sigma_{1500}^2 - \sigma_0^2 \qquad (A4)$$

where σ_{1500} is the RMS of the pedestal distribution of a given channel at 1500 Volts operating voltage and σ_0 the RMS without operating voltage. Since this noise is caused by the natural radioactivity of the uranium absorber and the total amount of charge collected due to radiation picked up by a pad is proportional to the pad area(A) times integration time(τ), the noise is expected to scale with $\sqrt{A\tau}$. The integration time τ was 3.5μs. Using all channels and the 50 GeV electron scale from Load III, it was found that:

$$\sigma_U = 0.12\ \frac{\sqrt{A\,\tau}}{SF} \qquad [MeV] \qquad (A5)$$

The statistical error is of order 1% and the units for A and τ are [m^2] and [nsec] respectively. These results were very well reproduced in Load II, as well as in a subsequent built copper-uranium mixture where only one side of a pad faced uranium. Moreover, during the end of the data taking for Load III, the argon was doped with Allene[12], resulting in a 70% increase in the α-test source signal, but no statistically significant increase or decrease in the beam related signals was observed. The uranium noise increased by 8%. This implies that the contribution of heavily ionizing fragments to uranium noise plays only a small role.

All of the above results were obtained by drifting the electrons released in the argon

towards the readout boards. By reversing the operating field (electrons drift towards absorber plates), the uranium noise ($\sigma_U{}^R$) was remeasured and decreased by the ratio

$$\sigma_U{}^R / \sigma_U = .74 \qquad \text{(A6)}$$

in good agreement with reference [13]. Based on this it was decided to operate future D0 calorimeters in this way, in order to minimize the uranium noise. Using equation (A5) for the uranium noise, the expected value in the different sections of the test calorimeter were: electromagnetic-section: 280 MeV, fine hadronic section: 980 MeV, electromagnetic + fine hadronic: 1.02 GeV.

To determine independently the contribution of noise to the resolution pedestal events were analyzed in the same way as regular events(pedestal subtraction, gain correction, sampling fraction weighting). Again the 50 GeV energy scale was used to convert from counts to beam energy, but now the electron scale was used for the electromagnetic-section only and the hadronic scale for all other sections. Table VI summarizes the results. σ_{total} is the total measured noise defined in the same way as the resolution(s) and obtained by summing all channels in a section, without zero suppression. $\sigma_{1\text{-}2}$ uses the same channels as σ_{total}, but instead of adding identical interleaved sections, they were subtracted. If there were no coherent contribution to the noise σ_{total} and $\sigma_{1\text{-}2}$ should be identical; if coherent noise did exist, it would be given by:

$$\sigma_{coh}{}^2 = \sigma_{total}{}^2 - \sigma_{1\text{-}2}{}^2 \qquad \text{(A7)}$$

This coherent noise is obviously the dominant noise source in every section of the calorimeter. In an independent analysis, carried out with the operating voltage turned off to minimize the effect of the uranium noise, it was shown that this coherent noise is about 0.18/SF [MeV] per channel (independent of the channel capacitance). Furthermore it was shown that this noise scales linearly with the number of channels summed (unlike random noise which scales with the square root of the number of channels), which explains why this is the dominent noise source despite the small per channel contribution.

The total incoherent (random) noise ($\sigma_{1\text{-}2}$) is a sum of the random electronic and

uranium noise:

$$\sigma_{1\text{-}2}^2 = \sigma_U^2 + \sigma_{\text{el. rand}}^2 \qquad \text{(A8)}$$

Assuming the uranium noise as calculated above, good agreement was found between the predicted values for the random electronic noise using equation (A1) and the results from (A8) as shown in Table VI.

TABLE VI

Noise as measured and calculated in different sections of the calorimeter in units of MeV.

Section	σ_{total}	$\sigma_{1\text{-}2}$	σ_{coh}	σ_{U}	$\sigma_{el.}$
electromagnetic(em)	760	325	687	280	165
fine hadron(fh)	1621	1078	1206	1045	265
leakage	679	378	564	---	378
em + fh	1984	1116	1641	1084	265
all added	2456	1184	2147	1084	476

References

1. W.J. Willis and V. Radeka, Nucl. Inst. and Meth. 120, (1974), 221. C.W. Fabjan et. al., Nucl. Inst. and Meth. 141, (1977), 61
2. V. Radeka, IEEE Trans. Nucl. Sci NS-21, 1 (1974) 51
3. R.Wigmans, Nucl. Inst. and Meth. A259 (1987) 389
4. H. Abramowicz et. al., Nucl. Inst. and Meth. 180, (1981), 429.
5. Review of Particle Properties, Physics Letters 170B, (1986), 1.
6. W. Lohmann, CERN/EP 85-03.
7. E. Longo and I. Sestilli, Nucl. Inst. and Meth. 128, (1975), 283. See also U. Amaldi, Physica Scripta 23, (1981), 409.
8. G. Barbiellini et al., CERN/EP 84-146 (1984).
9. R. Engelmann et. al., Nucl. Inst. and Meth. 216, (1983), 45.
10. R. Bock et al., Nucl. Inst. and Meth. 186, (1981), 533.
11. P.Franzini , Internal D0-notes.
12. D.F. Anderson, Nucl. Inst. and Meth. A245 (1986), 361.
13. N.D. Giokaris et .al., Nucl. Inst. and Meth. A248, (1986), 389.
14. G.A. Akopdjanov et. al., Nucl. Inst. and Meth. 140, (1977), 441
15. S.Stampke, Internal D0-note 396.
16. L.Bugge, Nucl. Inst. and Meth. A242, (1986), 228

FIGURE CAPTIONS

1. Transverse segmentation of the readout board.
2. Schematic view of the readout electronics .
3. (a) High voltage curve for Load II configuration using 50GeV electrons and hadrons.

   (b) High voltage curve for Load III configuration using 50GeV electrons and hadrons.
4. (a) Linearity of electron and hadron response in Load II configuration without any cuts.

   (b) Linearity of electron and hadron response in Load III configuration with and without the standard cuts.
5. (a) Energy resolution for electrons in Loads II and III without any cuts.

   (b) Energy resolution for electrons in Load III under different conditions.

   A) no cuts B) with 1.5σ cut C) interleave difference no cuts

   D) interleave difference with 1.5σ cut.
6. (a) Energy resolution for hadrons in Load II and III without any cuts.

   (b) Energy resolution for hadrons in Load III under different conditions.

   A) no cuts B) with 1.5σ cut C) interleave difference no cuts

   D) interleave difference with 1.5σ cut.
7. (a) Spectrum of 25GeV electrons observed in Load III with the 1.5σ cut.

   (b) Spectrum of 25GeV hadrons/muons observed in Load III with the 1.5σ cut.
8. (a) Containment of hadron showers as a function of the calorimeter depth used.

   (b) Hadron energy resolution as a function of the calorimeter depth used.
9. The ratio of electron over hadron response(e/h) in both configurations. Load II data are without any cuts. Load III data with and without cuts agree to within 1%. The lines drawn are simply connecting the data points.

10. The longitudinal profile of electrons as a function of energy. Experimental errors on the data are of the order of the size of the points. The curve is the best fit to the data as described in the text.

11. The energy dependence of parameters α and b used in describing the longitudinal profile of electrons in the calorimeter.

12. Differential transverse electron shower profile from lead pickup in segment EM3 for 150Gev electrons.

13. Ratios $G(x_b)$ at 50GeV for the four electromagnetic segments. The pad edge is at $x_b=0$. The solid curves are the double exponential fits.

14. Energy dependence of electron transverse shower shape parameters in EM3. a)A_1/E_T and A_2/E_T, b)B_1 and B_2.

15. Position resolution at 15,50 and 150GeV for electrons as a function of x_b, the distance between beam impact point and pad edge.

A1. Measured random electronic noise as a function of the cell capacitance and superimposed the linear fit.

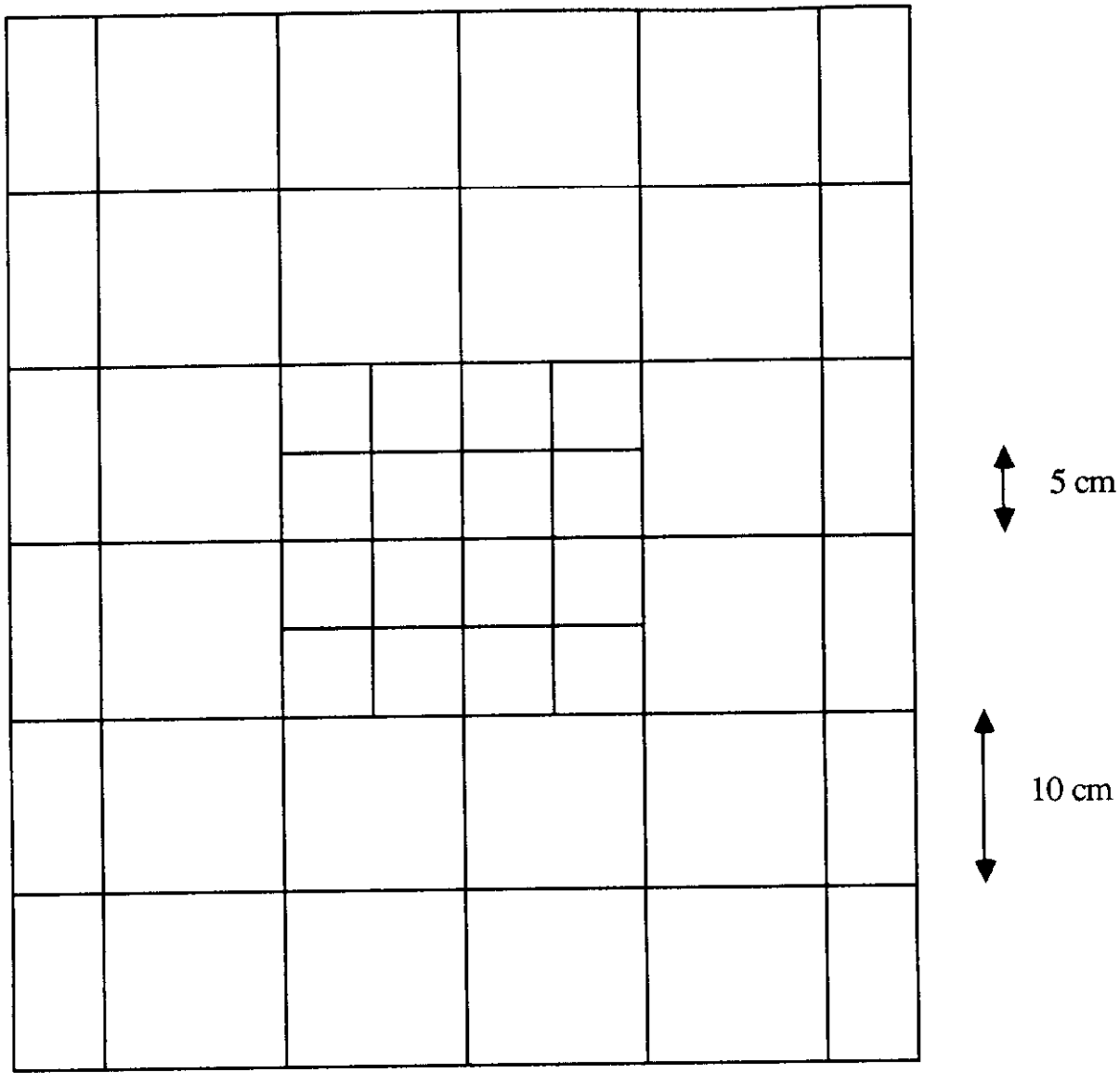

Fig. 1 Transverse segmentation of readout board.

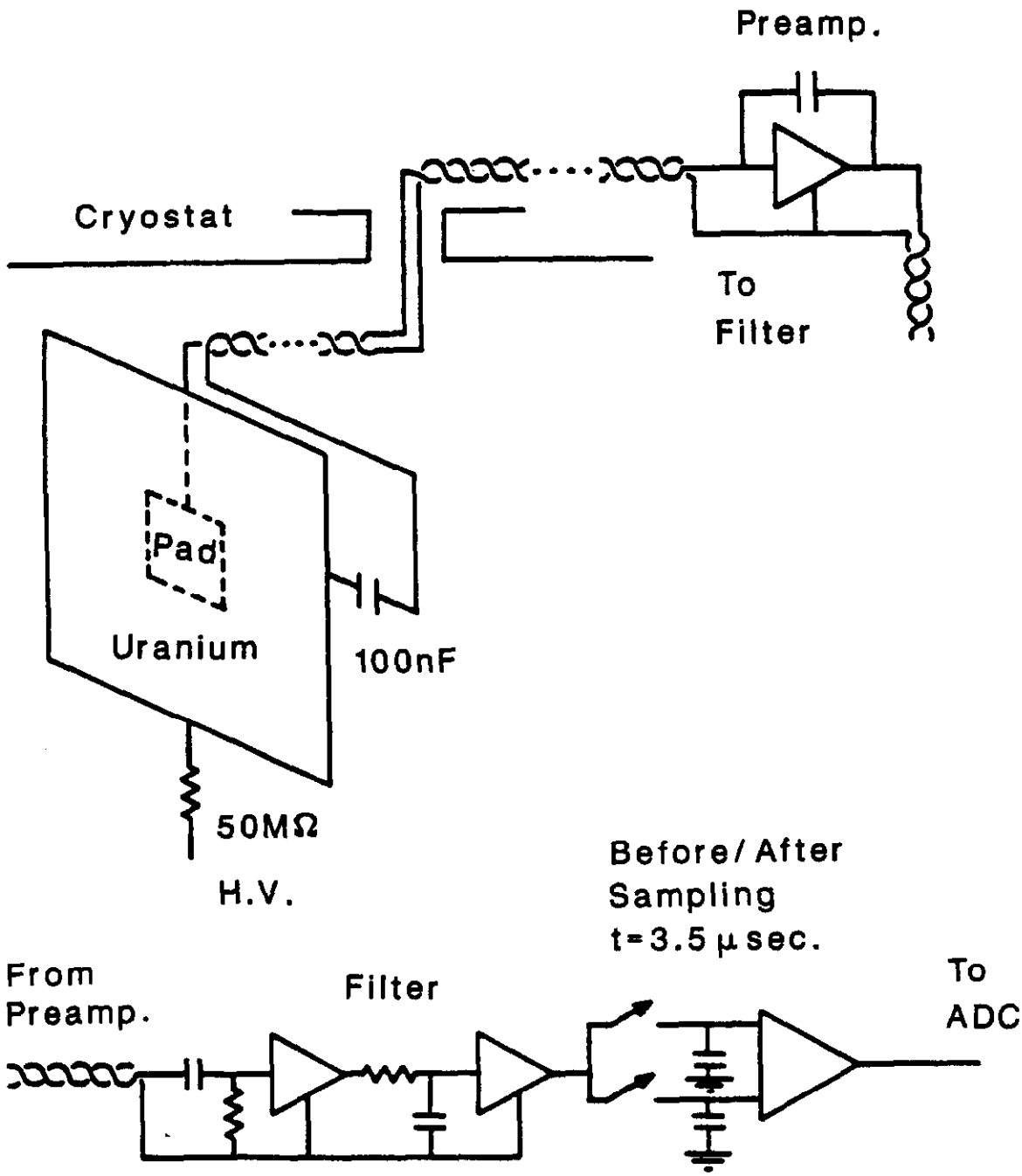

Fig. 2. Schematic view of the readout electronics.

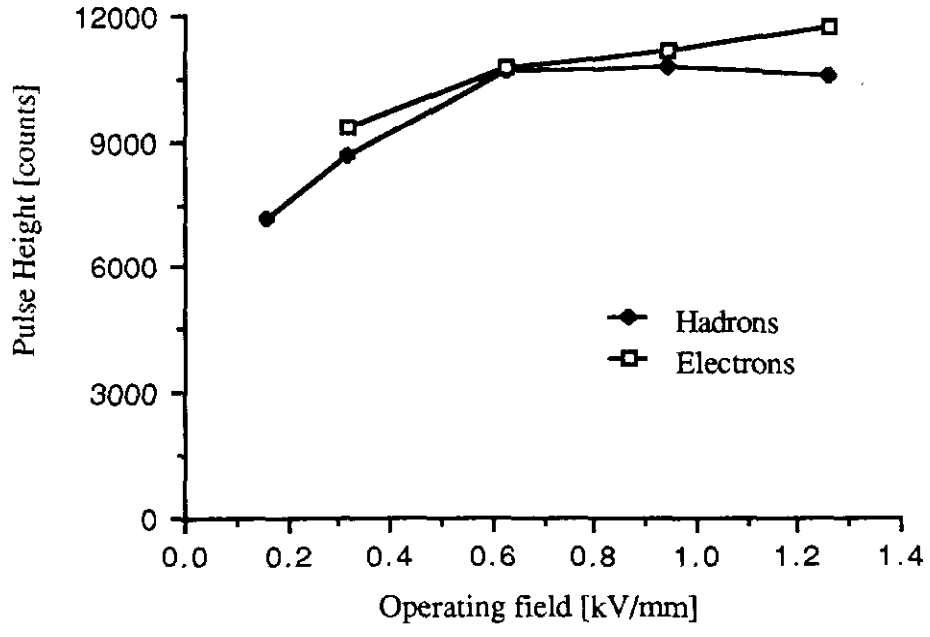

Fig. 3a. High voltage curve for Load II configuration using 50GeV electrons and hadrons.

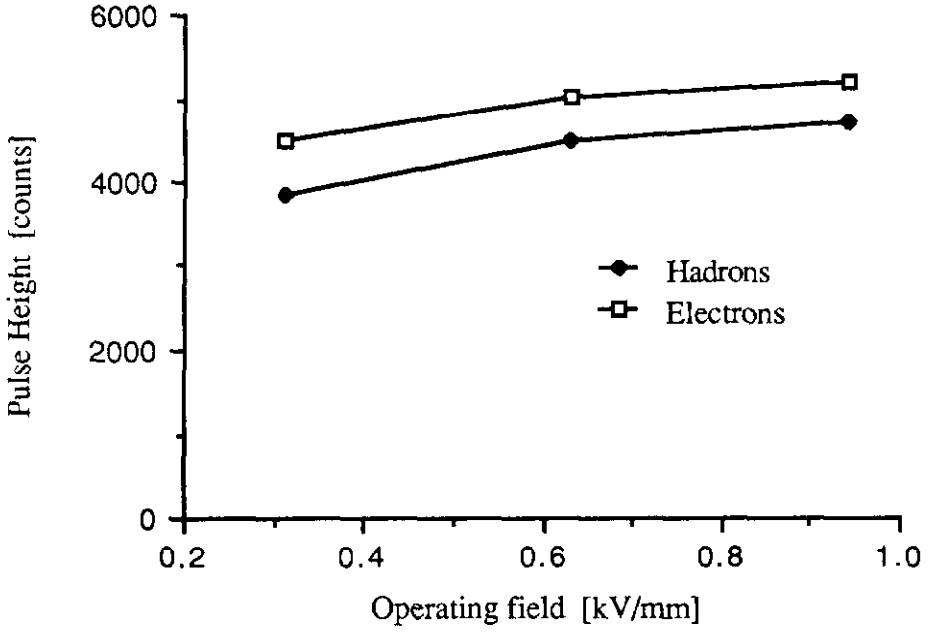

Fig. 3b. High voltage curve for Load III configuration using 50GeV electrons and hadrons.

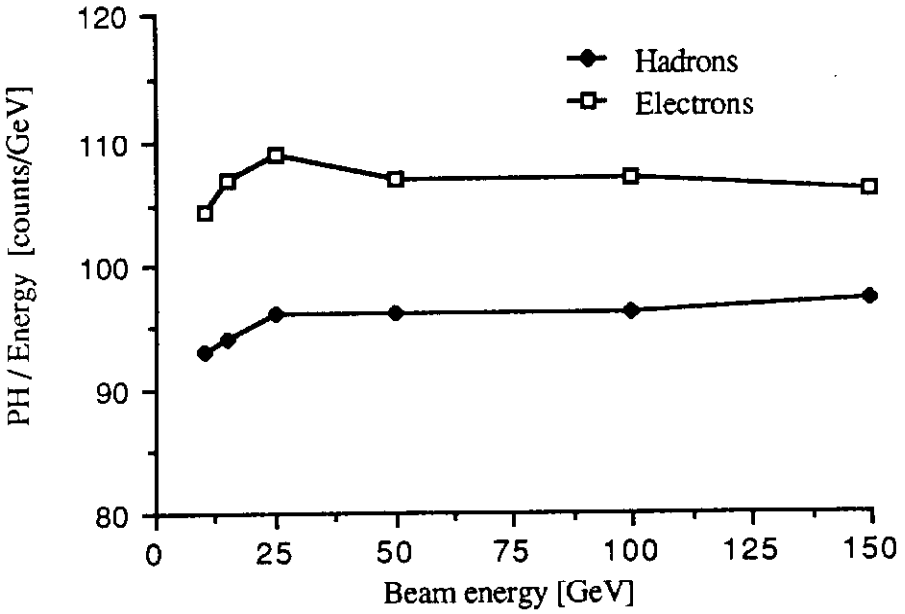

Fig. 4a. Linearity of electron and hadron response in Load II configuration without any cuts.

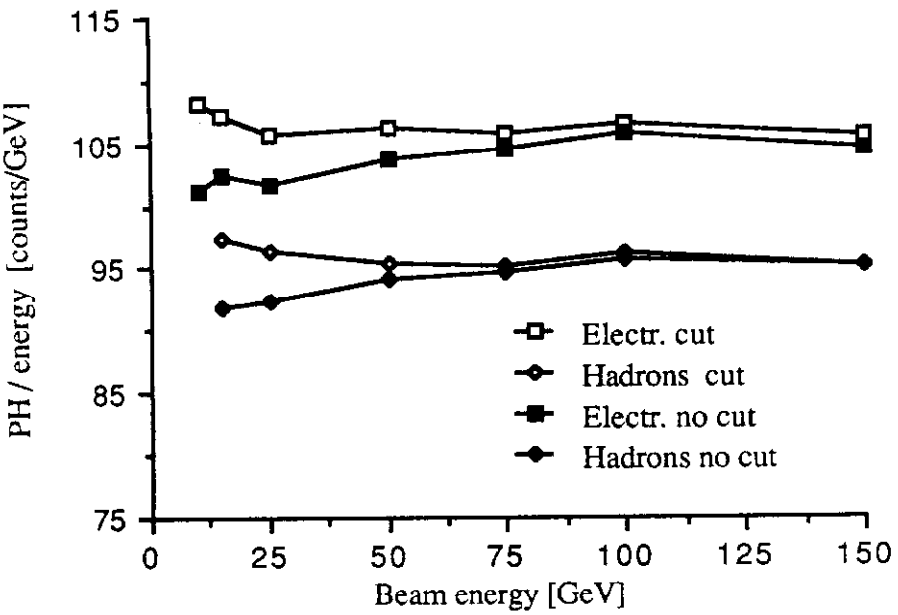

Fig. 4b. Linearity of electron and hadron response in Load III configuration with and without the standard cuts.

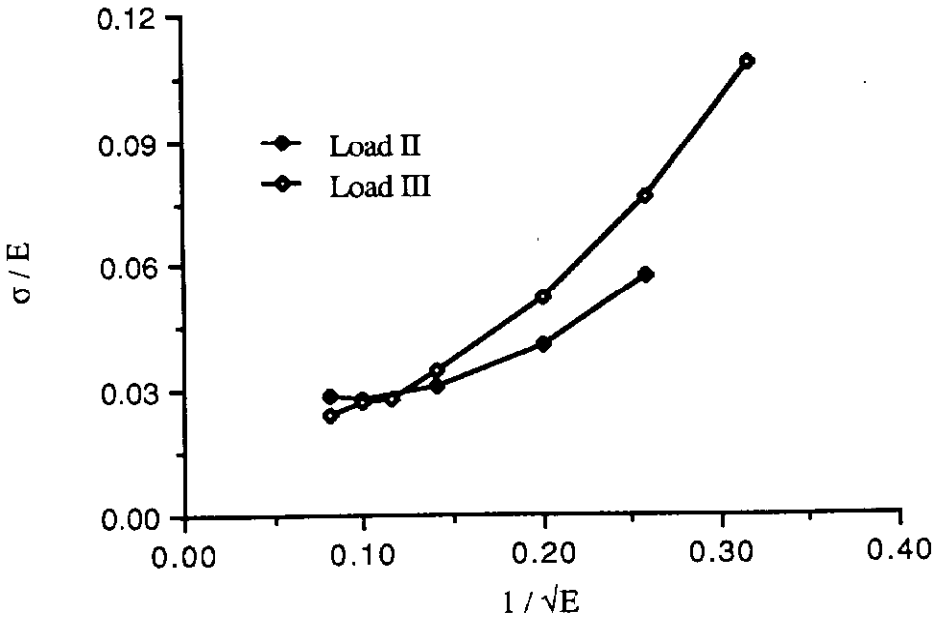

Fig. 5a. Energy resolution for electrons in Loads II and III without any cuts.

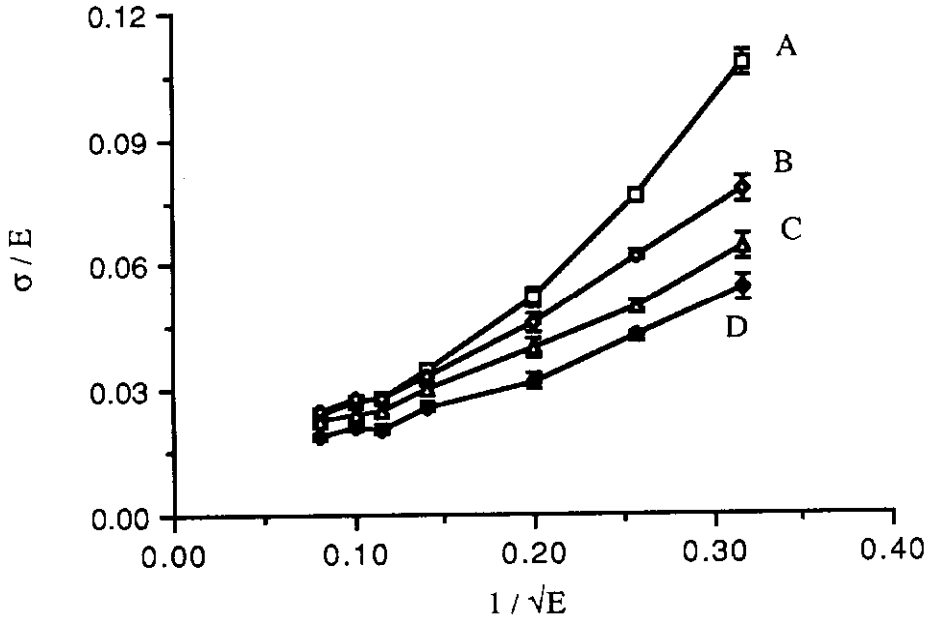

Fig. 5b. Energy resolution for electrons in Load III under different conditions:
A) no cuts B)with 1.5sigma cut C)interleave difference no cuts
D) interleave difference with 1.5sigma cut.

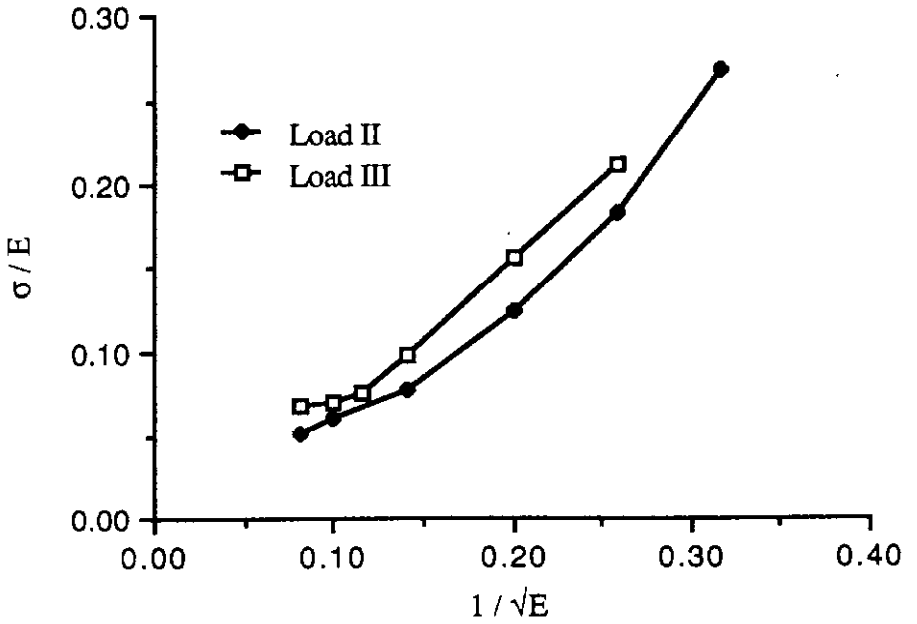

Fig. 6a. Energy resolution for hadrons in Loads II and III without any cuts.

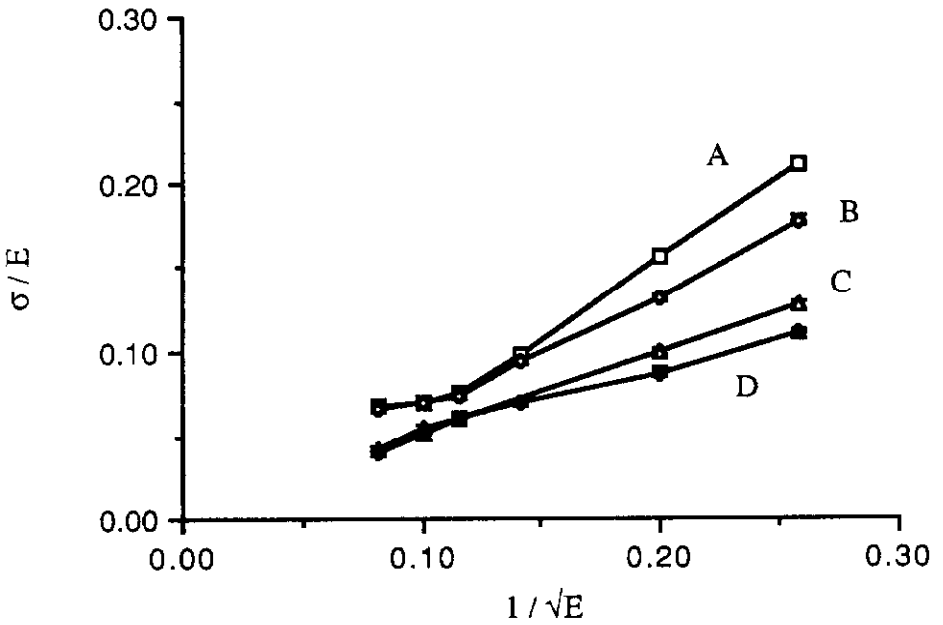

Fig. 6b. Energy resolution for hadrons in Load III under different conditions:
A) no cuts B)with 1.5sigma cut C)interleave difference no cuts
D) interleave difference with 1.5sigma cut.

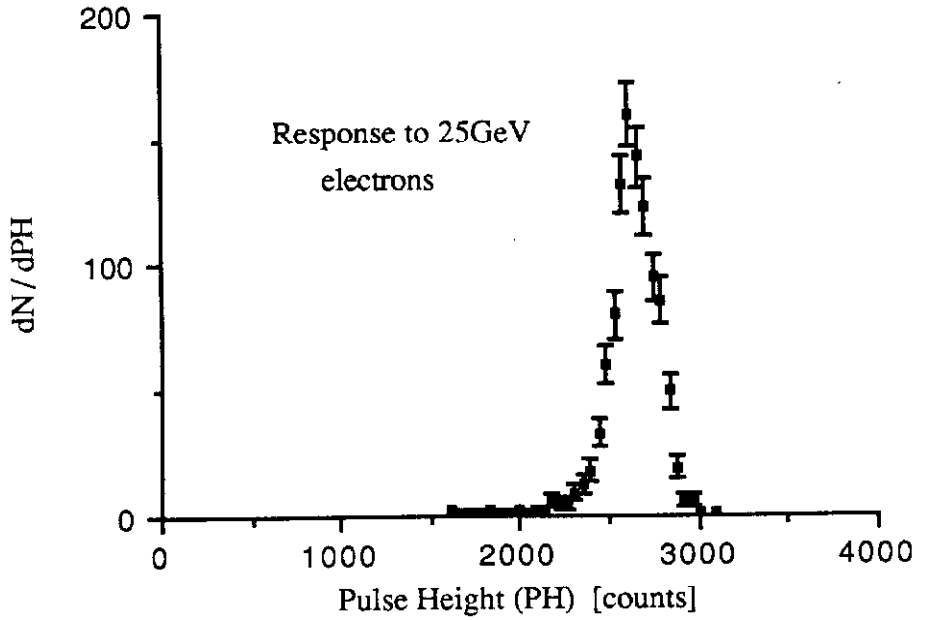

Fig. 7a. Spectrum of 25GeV electrons observed in Load III with the 1.5sigma cut.

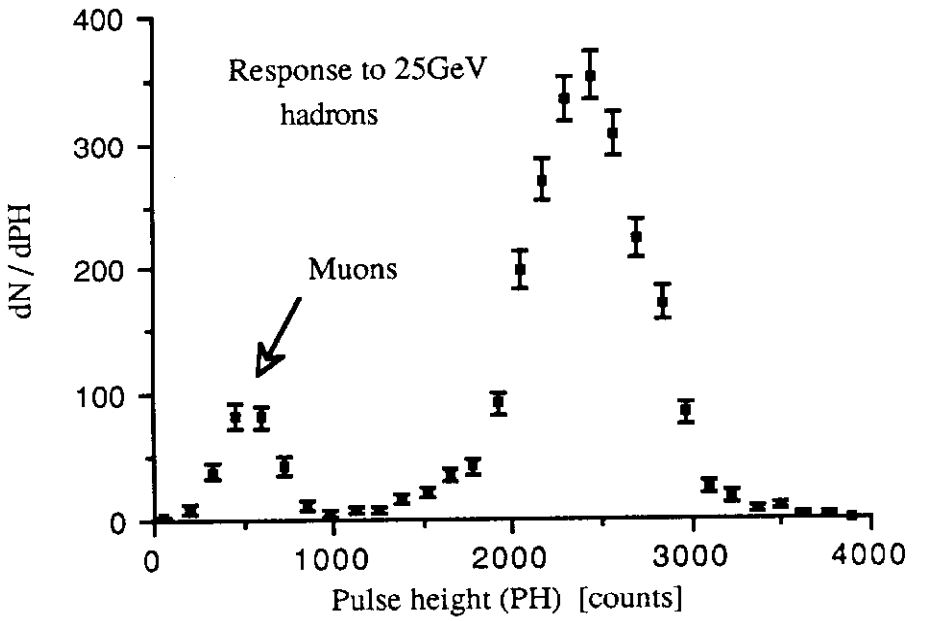

Fig. 7b. Spectrum of 25GeV hadrons observed in Load III with the 1.5sigma cut.

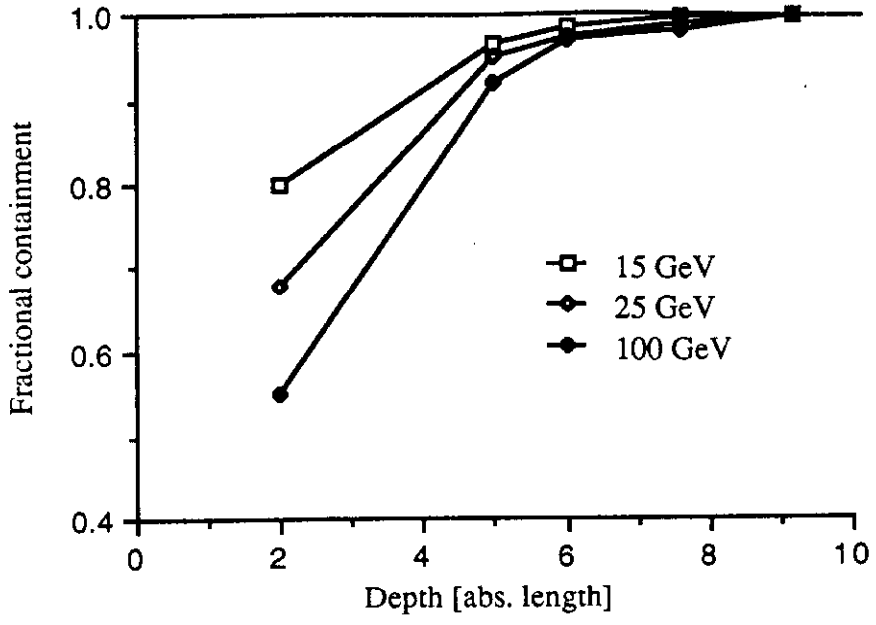

Fig. 8a. Containment of hadron showers as a function of the calorimeter depth used.

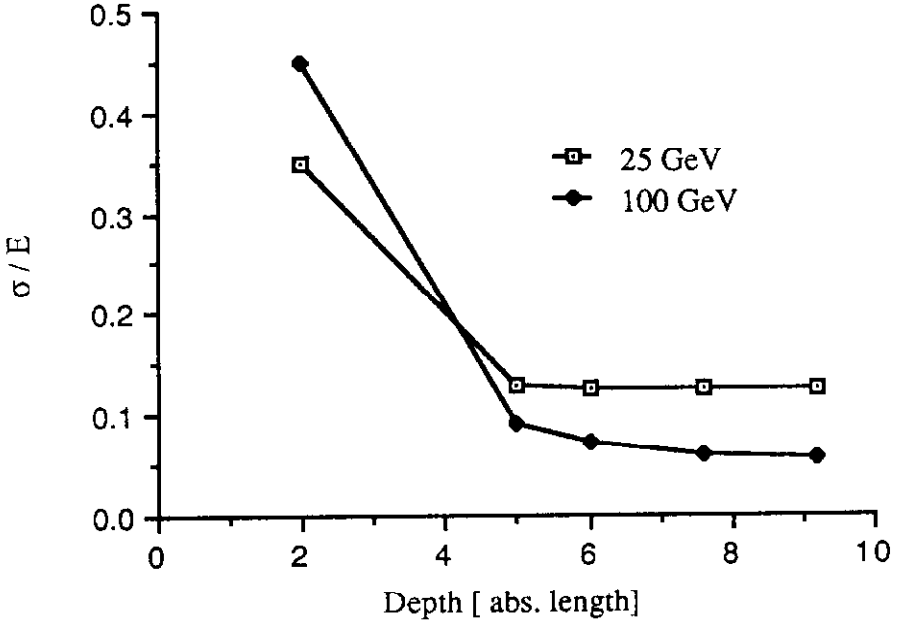

Fig. 8b. Hadron energy resolution as a function of the calorimeter depth used.

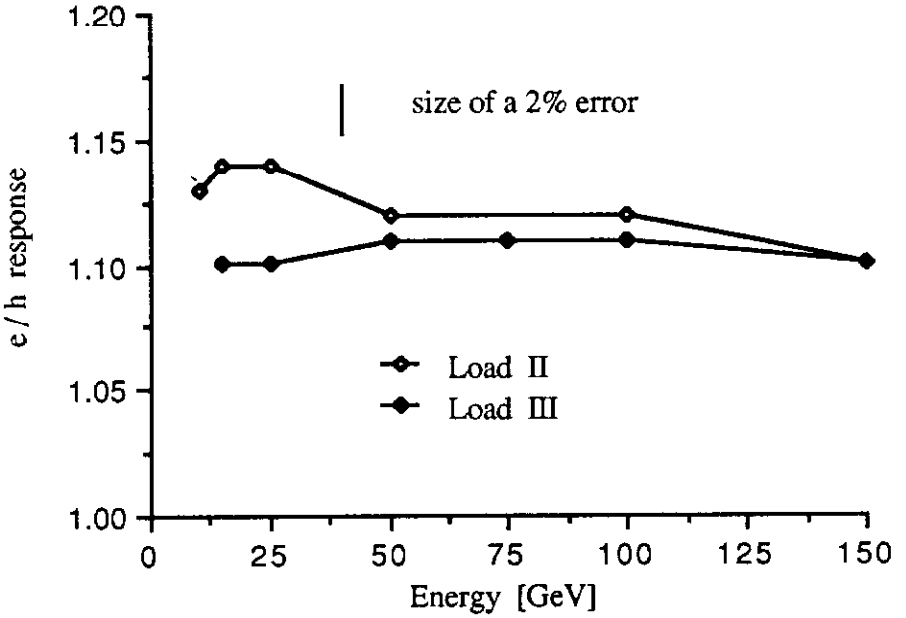

Fig. 9. The ratio of electron over hadron response (e/h) in both configurations. Load II data are without any cuts. Load III data with and without cuts agree to within 1%. The lines drawn are simply connecting the data points.

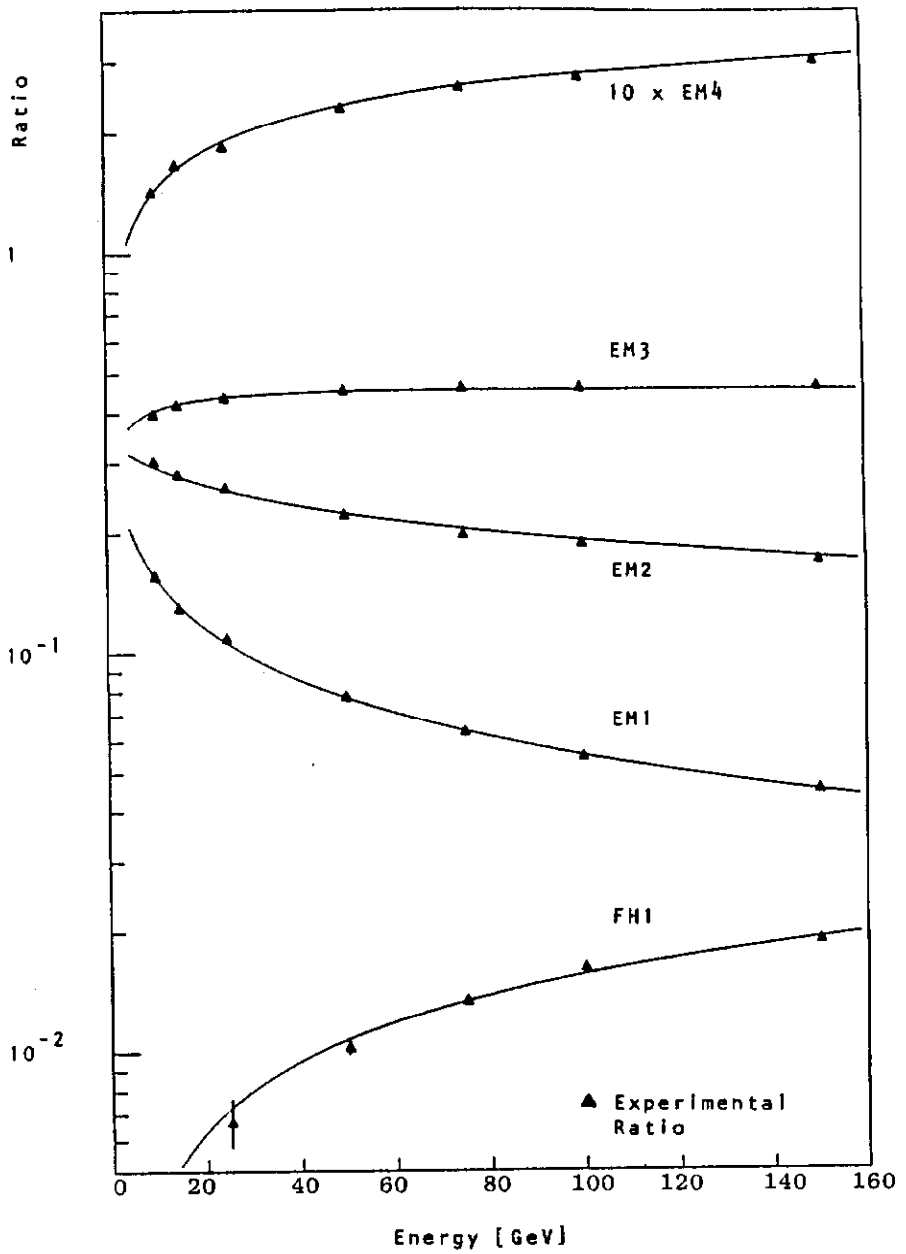

Fig.10. The longitudinal profile of electrons as a function of energy. Experimental errors on the data are of the order of the size of the the points. The curve is the best fit to the data as described in the text.

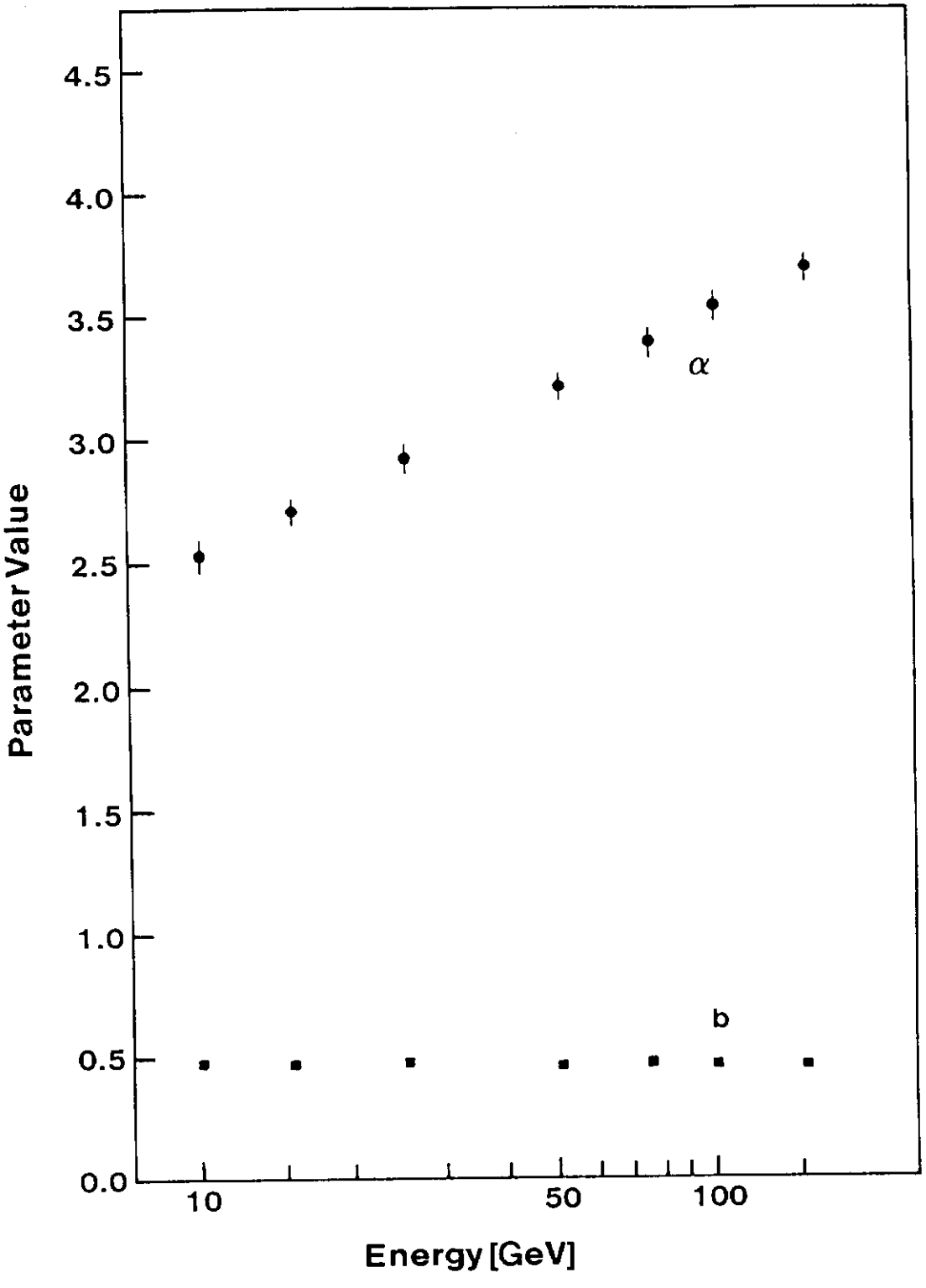

Fig. 11. The energy dependence of parameters α and b used in describing the longitudinal profile of electrons in the calorimeter.

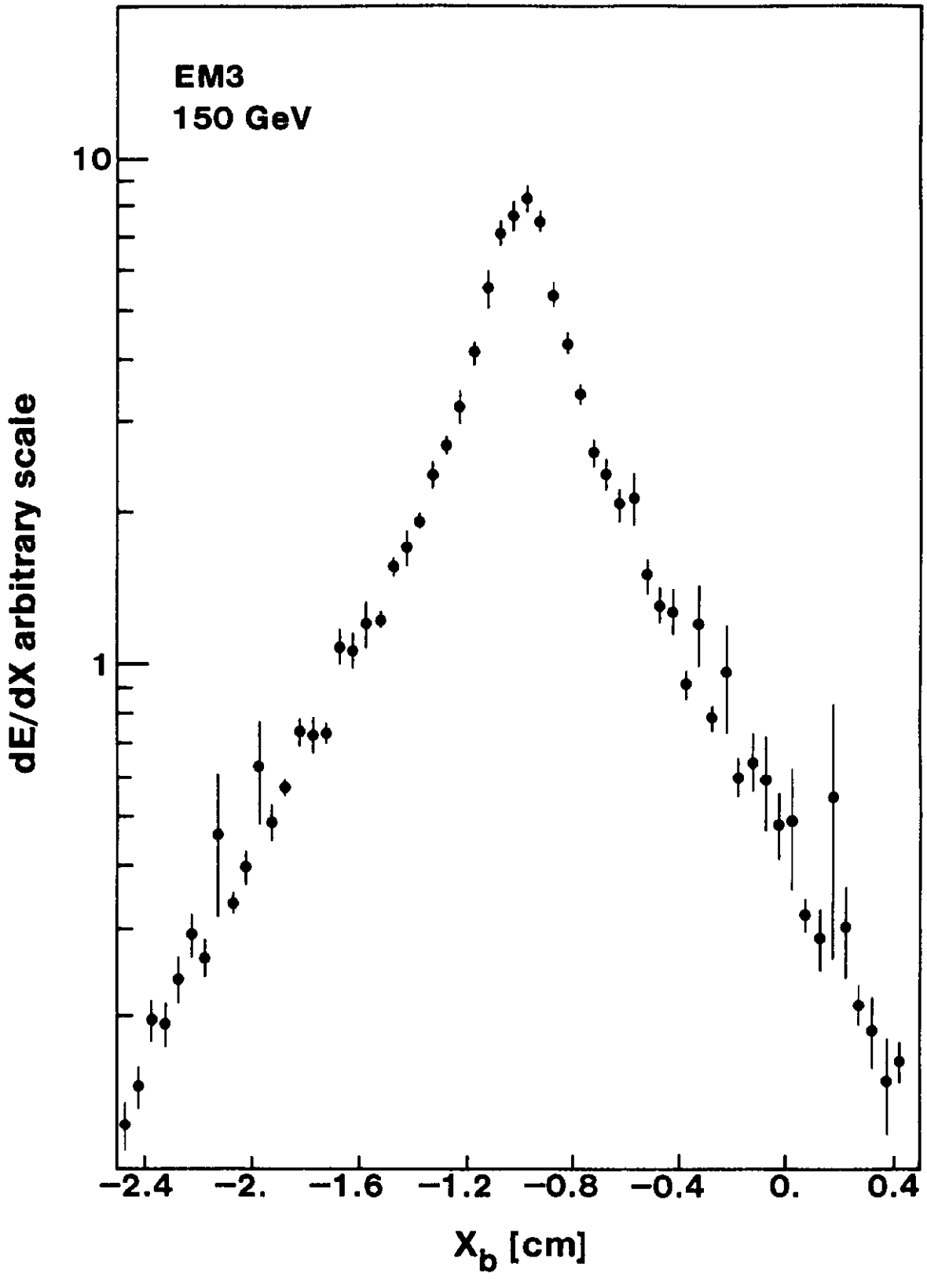

Fig.12. Differential transverse electron profile from lead pickup in segment EM3 for 150GeV electrons.

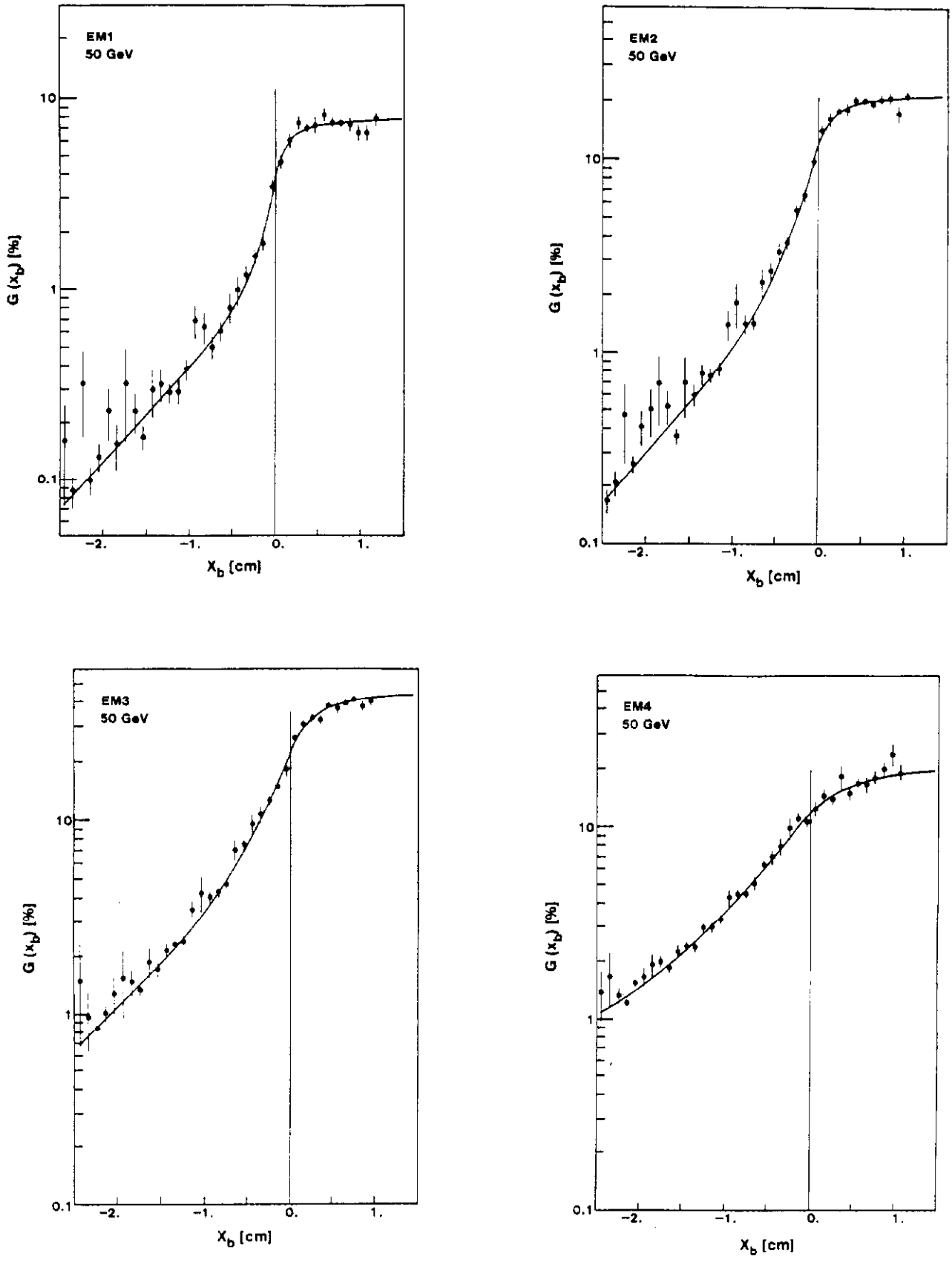

Fig. 13. Ratios G(x_b) at 50GeV for the four electromagnetic segements. The pad edge is at x_b =0. The solid curves are the double exponential fits.

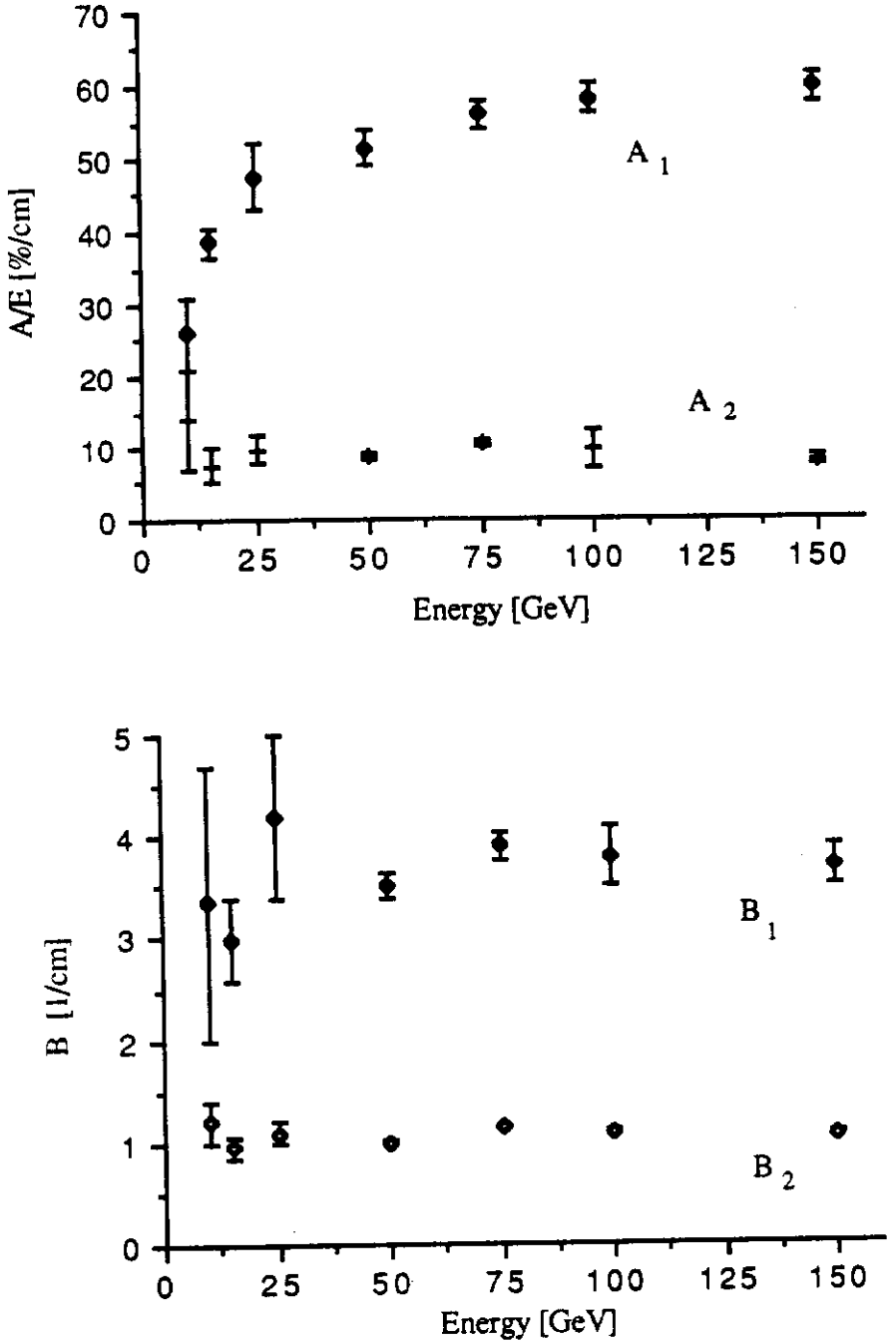

Fig. 14. Energy dependence of electron transverse shower shape parameters in EM3.
a) A_1 / E_T and A_2 / E_T, b) B_1 and B_2

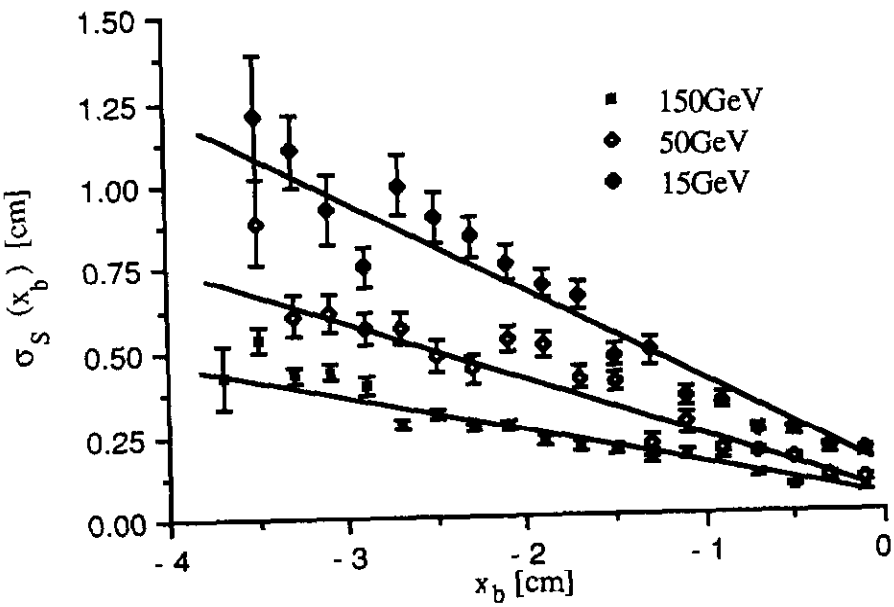

Fig. 15. Position resolution at 15, 50 and 150GeV for electrons as a function of x_b, the distance between beam impact point and pad edge.

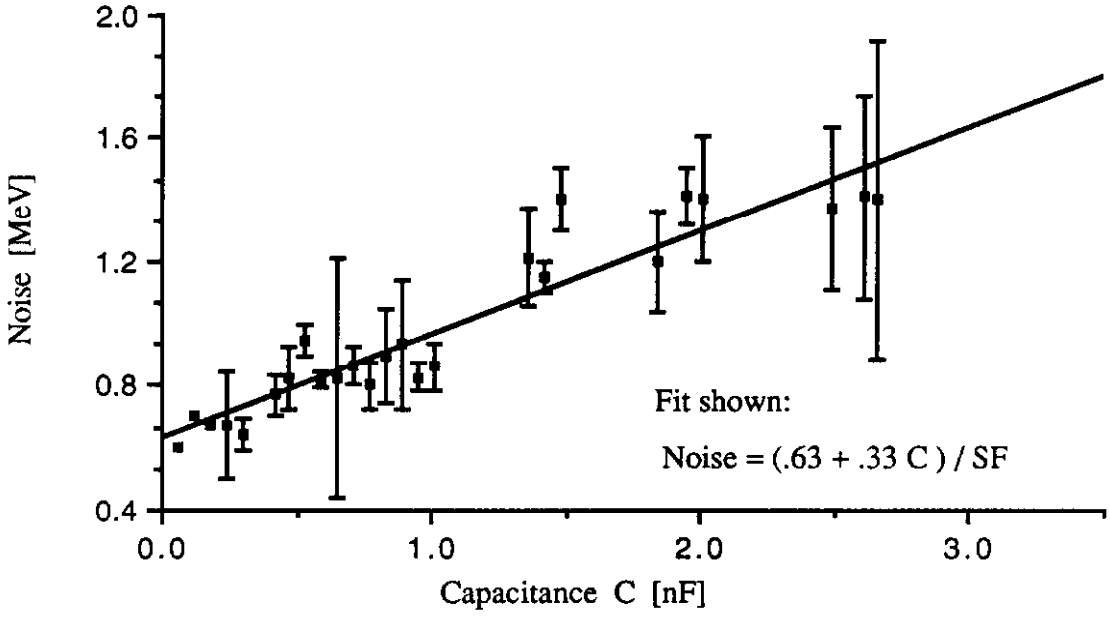

Fig. A1. Measured random electronic noise as a function of the cell capacitance and superimposed the linear fit.